Optics Letters

Wide field-of-view angle linear retarder with an ultra-flat retardance response

Honggang Gu,[1] Xiuguo Chen,[1,2] Hao Jiang,[1] Yating Shi,[1] and Shiyuan Liu[1,3]

[1]State Key Laboratory of Digital Manufacturing Equipment and Technology, Huazhong University of Science and Technology, Wuhan, Hubei 430074, China
[2]e-mail: xiuguochen@hust.edu.cn
[3]e-mail: shyliu@hust.edu.cn

Received 9 May 2019; accepted 10 May 2019; posted 15 May 2019 (Doc. ID 367259); published 7 June 2019

We propose a universal method for optimal design of a wide field-of-view (FOV) angle linear retarder with an ultra-flat retardance response based on paired positive/negative birefringent plates. The mechanism and rules for the FOV effect compensation are revealed to determine the structure of the proposed retarder by introducing the partial derivative of refractive index with respect to the incident angle. A concrete example based on quartz/sapphire plates is designed and manufactured as a proof-of-concept of the proposed method. The maximum deviation in the retardance of the optimally designed quartz/sapphire wide FOV angle retarder over the concerned FOV angles (incidence: –20°–20°; azimuth: 0°–360°) is only 0.08°, which has been reduced by 3 orders of magnitude compared with the common quartz retarder.

https://doi.org/10.1364/OL.44.003026

Linear retarders are basic elements to manipulate the polarized light by introducing a retardance between two polarized components in various optical systems, such as polarimetry and ellipsometry [1–3], interferometry [4,5], tomography [6], and microscopy [7,8]. The retardance of the retarder has significant influences on the final performance of related systems [9]. Any artifacts in retardance will degrade the precision of these systems [10–12]. Thus, in implementation of a high-precision optical system, the design of a stable retarder and accurate calibration of its retardance are of great importance.

Typical retarders include waveplates, Fresnel prisms, liquid crystal retarders, etc. A common retarder is usually designed for normal incidence, and its retardance exhibits a strong dependence on the field-of-view (FOV) angle (i.e., incidence and azimuth) of incident light [4,13,14]. Due to non-ideal collimation or improper installation and alignment in the practical optical path, the retarder is inevitably under an oblique incidence [4,9,13]. For example, in a polarimetric diagnosis system for immersion lithography with NA = 1.35, the incidence can be as large as ±20° [15]. For the wide FOV display systems, the incidence of light upon the retarder is even larger [16]. In these cases, the retardance will deviate away from its nominal value [13,17]. Thus, it is highly desirable to design a wide FOV angle linear retarder with a flat retardance response.

The most efficient way to obtain a wide FOV angle retarder is to find a material insensitive to incidence. Unfortunately, few natural materials can satisfy such a requirement. Although some emerging specially designed meta-structures can produce angle-insensitive polarization modulation, most of them are immature and usually used for long wavelengths [18,19]. Another strategy is to use positive and negative birefringent materials to compensate the FOV effect [16,20,21]. However, existing designs are usually obtained through empirical or exhaustive algorithms. They did not clarify the intrinsic mechanism and failed to give a general rule for the structure design, which makes them difficult to be extended to other designs for different applications or with more complicated structures.

Here, we start with discussing the FOV effect in birefringent materials, and the partial derivative of refractive index (RI) with respect to the incident angle is introduced to describe the changing rate of retardance within a birefringent plate. The mechanism and rules of the FOV effect compensation by using paired positive and negative birefringent plates are revealed. Finally, a universal and efficient method is proposed for the optimal design of a wide FOV angle linear retarder based on pairs of positive and negative plates.

Figure 1(a) shows the of light propagation in a birefringent plate at an oblique incidence. For convenience, the plate plane normal is chosen as the z-axis, and the optics axis is assumed to be parallel to the x-axis. In this case, the ordinary RI (oRI) remains unchanged, while the extraordinary RI (eRI) changes with the FOV angle of the incident light [17]

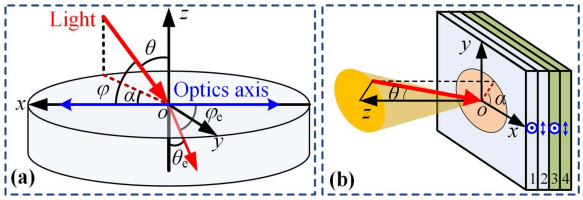

Fig. 1. (a) Light propagation in a birefringent wave at an oblique incidence; (b) proposed wide FOV retarder.

$$n = n_e\sqrt{1 + (1/n_e^2 - 1/n_o^2)\cos^2\varphi}, \quad (1)$$

where, n_e and n denote the eRIs at normal and oblique incidences, n_o is the oRI, and φ is the FOV angle. According to Fig. 1(a), we have $\cos\varphi = \sin\theta \cdot \cos\alpha$, where θ and α are the incidence and the azimuth of the incident light, respectively.

The changing eRI will further lead to varying retardance versus the FOV angle. This phenomenon is known as the FOV effect of a birefringent waveplate. In general, the birefringence (i.e., $\Delta n = n_e - n_o$) is much smaller than the eigen RIs (i.e., n_e and n_o). In this case ($\Delta n \ll n_e$ and n_o), the changing rate of retardance versus the incidence can be represented by

$$\delta' = \frac{\partial\delta}{\partial\theta} = \frac{2\pi}{\lambda}\frac{d}{\cos\theta_e}\cdot n' = \frac{2\pi}{\lambda}\frac{n}{\sqrt{n^2 - \sin^2\theta}}\cdot d\cdot n'. \quad (2)$$

Here, θ_e and d are the refraction angle of the e-ray and the plate thickness, respectively, and n' is the partial derivative of the eRI with respect to the incidence, which is defined as

$$n' = \frac{\partial n}{\partial\theta} = \frac{n_o^2 - n_e^2}{2n_o^2 n}\cos^2\alpha\sin 2\theta. \quad (3)$$

It can be seen from Eqs. (2), (3) that the retardance change for a positive plate ($n_e > n_o$) has an opposite direction with that of a negative plate ($n_e < n_o$). Thus, combining positive and negative plates is able to compensate the FOV effect. In this combination, plates that introduce the target retardance are named as retarding plates, while those used to compensate the retardance deviation are called compensating plates. To completely compensate the FOV effect, each retarding plate should be paired with a compensating plate, and the retardance changing rates should satisfy $\delta_c' = -\delta_r'$. Accordingly, we have

$$\frac{d_r}{d_c} = \frac{n_{or}^2(n_{ec}^2 - n_{oc}^2)}{n_{oc}^2(n_{or}^2 - n_{er}^2)}\frac{\sqrt{n_r^2 - \sin^2\theta}}{\sqrt{n_c^2 - \sin^2\theta}}, \quad (4)$$

where, the subscripts "r" and "c" represent the retarding plate and the compensating plate, respectively.

Equation (4) provides a basic and universal metric to design a wide FOV angle waveplate. When the incident angle is within a small range, the right part of Eq. (4) approximates to a constant for a certain wavelength. Table 1 gives the results for an incidence range of −20°–20° for several typical birefringent crystals, including quartz, MgF_2, and sapphire. RIs of these materials are from Refs. [22–24].

Inspired by the above theory and analysis, we can design a wide FOV angle linear retarder by combining paired positive/negative birefringent plates. Figure 1(b) illustrates the structure of a typical example, which consists of four single plates. Two of them are the retarding plates (numbered as 1 and 2), composing a compound zero-order waveplate with a target retardance δ_0. While the other two (numbered as 3 and 4) are compensating plates, composing a compound zero-order waveplate with 0-retardance. Therefore, the thicknesses of these single plates have the following relations

Table 1. Results of Eq. (4) for Quartz, $MgF_{2(m)}$, and Sapphire(s)

Wavelength (nm)	193	325	532	633	800
d_q/d_s	1.598[a]	1.488	1.477	1.474	1.468
d_m/d_s	2.179	2.342	2.399	2.406	2.408

[a]Data are mean results for Eq. (4) in an incidence range of −20°–20°.

$$d_1 - d_2 = \frac{\delta_0\lambda}{2\pi(n_{er} - n_{or})}, \qquad d_3 - d_4 = \frac{0\lambda}{2\pi(n_{ec} - n_{oc})}, \quad (5)$$

where, d_i ($i = 1, 2, 3, 4$) is the thickness of the ith single plate, n_{er} (n_{ec}) and n_{or} (n_{ec}) are eRI and oRI for retarding (compensating) plates, respectively, and λ is the wavelength. In addition, the thicknesses of the plates satisfy Eq. (4), where $d_r = (d_1 + d_2)/2$ and $d_c = (d_3 + d_4)/2$.

Combining Eqs. (4), (5), we can determine an initial structure for the proposed wide FOV retarder. To further obtain the optimal design, we can minimize the maximum deviation from the target retardance over the whole desired FOV

$$\mathbf{d}_o = \arg\min_{\mathbf{d}\in[\mathbf{d}_0-\Delta d,\,\mathbf{d}_0+\Delta d]}\left[\max_{\theta\in[-\theta_0,\theta_0],\,\alpha\in[0,360^\circ]}(|\delta - \delta_0|)\right], \quad (6)$$

herein, $\mathbf{d} = [d_1, d_2, d_3, d_4]$ refers to the thickness set for the single plates, $\mathbf{d_0} = [d_{10}, d_{20}, d_{30}, d_{40}]$ and $\mathbf{d_o} = [d_{1o}, d_{2o}, d_{3o}, d_{4o}]$ are initial thicknesses and the optimal thicknesses, respectively, Δd is a small value to define the optimization interval for the thicknesses, θ_0 is the maximum incident angle, δ_0 is the target retardance, and δ is the retardance of the proposed retarder at an arbitrary incidence θ and azimuth α, which can be strictly calculated by [17]

$$\delta = \frac{2\pi}{\lambda}\sum_{i=1}^{4}\left[(-1)^{i+1}d_i\left(\sqrt{n_i^2 - \sin^2\theta} - \sqrt{n_{oi}^2 - \sin^2\theta}\right)\right], \quad (7)$$

where, n_i and n_{oi} are eRI and oRI of the ith plate at arbitrary FOV angle, respectively, and n_i can be calculated by Eq. (1).

A wide FOV angle quarter-wave retarder at the wavelength of 633 nm using quartz/sapphire plates is presented as a concrete example to verify the proposed methods. The maximum applicable incidence for the retarder is chosen as $\theta_0 = 20°$. Considering the challenges in processing (especially the thickness control), the sapphire plates (used as the compensating plates) are first polished with a thickness of about 413 μm (i.e., $d_3 = d_4 = 413$ μm). Then, the quartz plates are manufactured with proper thicknesses to produce the target retardance and match the sapphire plates simultaneously. The thicknesses of quartz plates can be initially determined by Eqs. (4), (5). Further, we use the simulated annealing algorithm to do the optimization as described in Eq. (6) around the initial thicknesses with $\Delta d = 10$ μm; the final optimal thicknesses for the quartz plates are $d_1 = 288.10$ μm and $d_2 = 270.65$ μm. The choice of Δd depends on the birefringence and the maximum applicable incidence. The larger the birefringence and the incidence are, the larger Δd should be.

The retardance over the whole designed FOV can be evaluated by Eq. (7). Figure 2 shows the retardance of the optimally

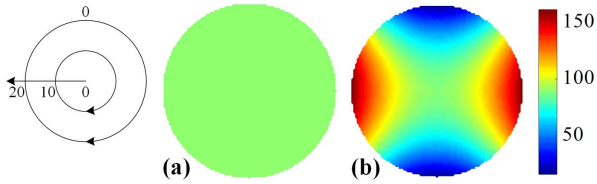

Fig. 2. Designed retardance: (a) optimal quartz/sapphire wide FOV angle retarder; (b) common quartz compound zero-order retarder. The polar axis and the polar angle denote the incidence (0–20°) and the azimuth (0–360°) of the light, respectively.

designed quartz/sapphire retarder and a common quartz compound zero-order retarder. The thicknesses of the single waveplates in the common retarder are designed as $d_1 = 288.10$ μm and $d_2 = 270.65$ μm. We can see that the common retarder exhibits large oscillation in retardance versus the FOV angle, and the oscillation amplitude drastically increases as the incidence increases. The maximum deviation in retardance of the common quartz retarder from the nominal value (90°) is larger than 72°. In comparison, the optimal wide FOV retarder exhibits an extremely flat retardance response over the whole FOV with a maximum deviation of about 0.08°, which has been reduced by about 3 orders of magnitude.

We have manufactured a quartz/sapphire wide FOV retarder in our laboratory according to the optimally designed structure. As stated above, the two compensating sapphire plates were first obtained through the same polishing process to ensure that they have equal thickness. After that, the retarding quartz plates were polished according to the optimal thicknesses. In order to perform a comparative experiment, additional copies of the quartz plates were polished in the same process to make a common compound zero-order retarder. Finally, all single plates were precisely aligned and cemented together with the help of a straight-through spectroscopic Mueller matrix ellipsometer (MME) and a high-precision automatic rotation stage [12], as shown in Fig. 3. The retarders were characterized on the same experimental platform based on MME over the whole designed FOV [25]. Figures 4 and 5 demonstrate the experimental results.

From Fig. 4, we can observe that the retardance distribution of the common quartz retarder is extremely uneven over the FOV with a maximum deviation of about 75° from the average value 90.94°. The waveform and amplitude of the oscillations

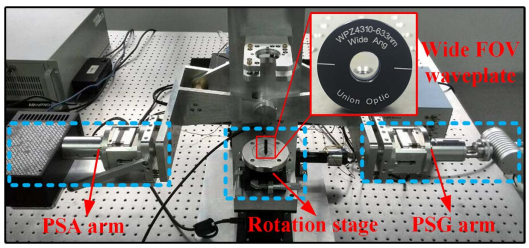

Fig. 3. MME experiment setup and the wide FOV waveplate.

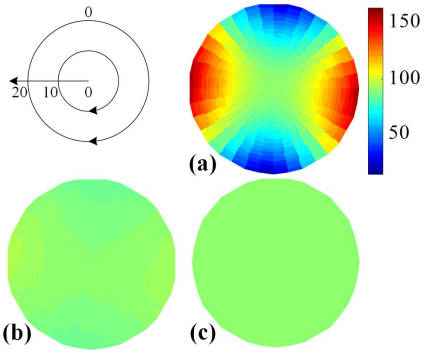

Fig. 4. Experimental retardance: (a) common quartz compound zero-order retarder; (b) polymer true zero-order retarder from Edmund; (c) quartz/sapphire wide FOV retarder.

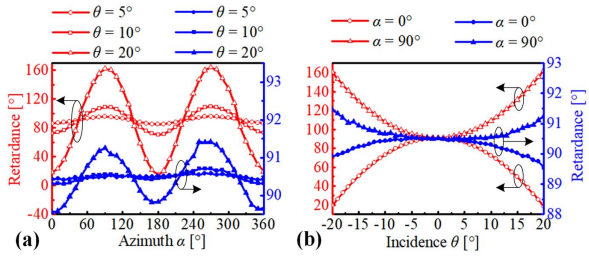

Fig. 5. Experimental retardance of the common quartz retarder (red solid lines with open marks) and the quartz/sapphire wide FOV retarder (blue solid lines with solid marks): (a) versus the azimuth of incident light; (b) versus the incidence of incident light.

highly agree with the theoretical results shown in Fig. 2(b). For the quartz/sapphire wide FOV angle retarder, although the retardance distribution is not as even as the optimally designed situation, the maximum deviation from the average value (90.49°) is about 0.95°, which is still much more stable than the common retarder. To further highlight the ultra-flat retardance response of our wide FOV angle retarder, a true zero-order retarder made of polymer (#49-220 from Edmund) with high-precision retardance over a wide incidence range, is also compared. As shown in Fig. 4(b), the high-precision polymer retarder has a maximum deviation of over 5.95° from its average retardance (89.87°) over the whole FOV, which is over 6 times larger than that of our quartz/sapphire wide FOV retarder. It should be pointed out that although the proposed quartz/sapphire retarder has a much flatter retardance response than the polymer zero-order retarder, its structure is more complicated, which may introduce more manufacturing errors.

To more clearly demonstrate retardance oscillations versus the incidence and azimuth, results in the polar images shown in Fig. 4 are replotted in the Cartesian coordinate system, as shown in Fig. 5. From Fig. 5(a), it can be seen that retardance exhibits sinusoidal-like oscillation versus the azimuth with a period of 180°. The peak-to-valley value (PVV) of the oscillation can be used to evaluate the stability of retardance from another point of view. The PVV of the wide FOV retarder is about two orders of magnitude smaller than that of the common retarder, verifying that the optimally designed wide FOV retarder has ultra-flat retardance. It is worth mentioning that the practical quartz/sapphire retarder appears asymmetric in retardance over the FOV. This weak asymmetry in retardance may be due to uneven sapphire plates, whose thickness uniformity over its aperture is hard to be guaranteed in the polishing process.

From Fig. 5(b), it can be observed that the retardance deviates away from the nominal value as incidence increases for both of the practical retarders. However, deviations in the quartz/sapphire wide FOV retarder are much smaller than those in the common quartz retarder. DC deviations of about 0.5° and 1° from the target value (90°) can be clearly found in the retardance of the wide FOV retarder and the common retarder, respectively. The DC deviations may come from errors in the thickness difference between the retarding plates. According to Eq. (5), the ideal value is $d_1 - d_2 = 17.45$ μm, and the errors are 0.10 μm and 0.19 μm, respectively, for the wide FOV retarder and common retarder. The practical quartz/sapphire retarder is undercompensated to the FOV effect

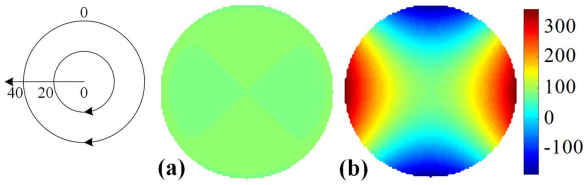

Fig. 6. Designed retardance: (a) optimal MgF_2/sapphire wide FOV retarder; (b) common MgF_2 compound zero-order retarder.

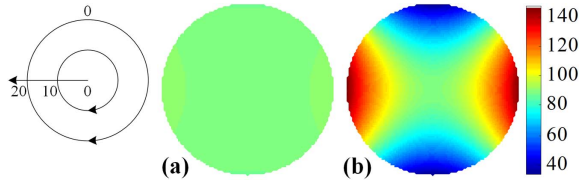

Fig. 7. Designed retardance: (a) optimal quartz/sapphire wide FOV multi-order retarder; (b) common quartz multi-order retarder.

compared with its optimal design, which is due to the thickness mismatch between the retarding and compensating plates.

To further demonstrate the validity of our method, two more examples are presented. The first one is an MgF_2/sapphire compound zero-order quarter-wave retarder at the wavelength of 633 nm used for an incidence range of –40°–40°. It has a similar structure with the quartz/sapphire retarder, containing two MgF_2 plates ($d_{m1} = 171.90$ μm and $d_{m1} = 158.47$ μm) and two sapphire plates ($d_{s1} = d_{s2} = 413$ μm). The second one is a quartz/sapphire multi-order quarter-wave retarder at the wavelength of 633 nm used for an incidence range of –20°–20°, containing a quartz plate ($d_q = 436.49$ μm) and a sapphire plate ($d_s = 642.14$ μm). Figures 6 and 7 show the retardance compared with their common forms. The maximum deviation in retardance of the MgF_2/sapphire retarder from its nominal value (90°) is 2.65°, compared with a maximum deviation of 271.80° in retardance of the common MgF_2 compound zero-order retarder. The maximum deviation in retardance of the quartz/sapphire multi-order retarder from the nominal value (90°) is about 1.23°, compared with a maximum deviation of 57.08° for the common quartz multi-order retarder.

In summary, we first investigated the mechanism and rules of the FOV effect of a birefringent plate. We found that the ratio of retardance changing rates of different crystals approximates to a constant versus FOV angles. Based on this, we proposed a strategy to design a wide FOV angle retarder using paired positive/negative birefringent plates. Thicknesses of all single plates are determined initially according to the ratio of retardance changing rates of the positive and negative birefringent plates. The structure of the wide FOV angle retarder is finally optimized by the simulated annealing algorithm. A wide FOV retarder based on quartz/sapphire plates is presented to verify the methods. Results demonstrate that the optimally designed quartz/sapphire retarder exhibits an ultra-flat retardance response over whole FOV with a maximum deviation of about 0.08° in retardance, which is reduced by about 3 orders of magnitude compared with that of the common quartz retarder.

It should be noted that the proposed method is universal and can be easily extended to design other types of wide FOV angle retarders. It is especially suitable for small birefringence within a small incidence range. It still works for giant birefringence under a large incident angle, but the initial thicknesses evaluated by Eq. (4) becomes less reliable with respect to the final optimal structure. In this case, a larger optimization interval (i.e., Δd) for the thicknesses should be used in Eq. (6) to guarantee to find the optimal design.

Funding. National Natural Science Foundation of China (NSFC) (51525502, 51727809, 51775217, 51805193); China Postdoctoral Science Foundation (2016M602288, 2017T100546); National Science and Technology Major Project of China (2017ZX02101006-004).

REFERENCES

1. T. Mu, C. Zhang, Q. Li, and R. Liang, Opt. Lett. **40**, 2485 (2015).
2. H. Gu, X. Chen, H. Jiang, C. Zhang, and S. Liu, J. Opt. **18**, 025702 (2016).
3. A. Messaadi, M. M. Sanchez-Lopez, A. Vargas, P. Garcia-Martinez, and I. Moreno, Opt. Lett. **43**, 3277 (2018).
4. D. Mawet, C. Hanot, C. Lenaerts, P. Riaud, D. Defrere, D. Vandormael, J. Loicq, K. Fleury, J. Plesseria, J. Surdej, and S. Habraken, Opt. Express **15**, 12850 (2007).
5. S. Danilishin, E. Knyazev, N. Voronchev, F. Khalili, C. Graf, S. Steinlechner, J. Hennig, and S. Hild, Light Sci. Appl. **7**, 11 (2018).
6. M. Villiger, B. Braaf, N. Lippok, K. Otsuka, S. Nadkarni, and B. Bouma, Optica **5**, 1329 (2018).
7. S. Pang, C. Han, M. Kato, P. Sternberg, and C. Yang, Opt. Lett. **37**, 5018 (2012).
8. O. Arteaga, M. Baldris, J. Anto, A. Canillas, E. Pascual, and E. Bertran, Appl. Opt. **53**, 2236 (2014).
9. E. West and M. Smith, Opt. Eng. **34**, 1574 (1995).
10. H. Dong, M. Tang, and Y. Gong, Opt. Express **20**, 26649 (2012).
11. H. Dai and C. Yan, Opt. Express **22**, 11869 (2014).
12. H. Gu, X. Chen, H. Jiang, C. Zhang, W. Li, and S. Liu, Appl. Opt. **55**, 3935 (2016).
13. P. Hale and G. Day, Appl. Opt. **27**, 5146 (1988).
14. C. Hsieh, R. Pan, T. Tang, H. Chen, and C. Pan, Opt. Lett. **31**, 1112 (2006).
15. H. Nomura, Thin Solid Films **519**, 2688 (2011).
16. Z. Ge, R. Lu, T. Wu, S. Wu, C. Lin, N. Hsu, W. Li, and C. Wei, Opt. Express **16**, 3120 (2008).
17. H. Gu, X. Chen, C. Zhang, H. Jiang, and S. Liu, J. Opt. **20**, 015401 (2018).
18. D. Lin, P. Fan, E. Hasman, and M. Brongersma, Science **345**, 298 (2014).
19. H. Shi and Y. Hao, Opt. Express **26**, 20132 (2018).
20. W. Kang, B. Mun, G. Lee, J. Lee, B. Kim, H. Choi, Y. Kim, and S. Lee, J. Appl. Phys. **111**, 103119 (2012).
21. Y. Furutono and H. Nomura, Opt. Rev. **16**, 188 (2009).
22. S. Chandrasekhar, Proc. Indian Acad. Sci. A **34**, 275 (1951).
23. M. Dodge, Appl. Opt. **23**, 1980 (1984).
24. I. Malitson and M. Dodge, J. Opt. Soc. Am. **62**, 1405 (1972).
25. H. Gu, X. Chen, Y. Shi, H. Jiang, C. Zhang, P. Gong, and S. Liu, Opt. Express **26**, 25408 (2018).